CRYSTAL GROWTH & DESIGN

Article

pubs.acs.org/crystal

Crystal Packing and Magnetism in Phenolic Nitronylnitroxides: 2-(3′,5′-Dimethoxy-4′-hydroxyphenyl)-4,4,5,5-tetramethyl-4,5-dihydro-1*H*-imidazole-1-oxyl

Gonca Seber,[†] Rafael S. Freitas,*[,‡] Nei Fernandes Oliveira, Jr.,[‡] and Paul M. Lahti*[,†]

[†]Department of Chemistry, University of Massachusetts, Amherst, Massachusetts 01003, United States

[‡]Instituto de Física, Universidade de São Paulo, C.P. 66318 - 05314-970 São Paulo, São Paulo, Brazil

Supporting Information

ABSTRACT: 2-(3′,5′-Dimethoxy-4′-hydroxyphenyl)-4,4,5,5-tetramethyl-4,5-dihydro-1*H*-imidazole-1-oxyl (SyrNN) forms a hydrogen bonded network of contacts involving phenolic OH and nitronylnitroxide methyl groups as donors, and nitronylnitroxide NO groups as acceptors. The SyrNN intermolecular contact network is quite similar to that of 2-(4′-hydroxyphenyl)-4,4,5,5-tetramethyl-4,5-dihydro-1*H*-imidazole-1-oxyl (HOPhNN) (Cirujeda et al., *J. Mater. Chem.* **1995**, *5*, 243−252), which shows ferromagnetic exchange interactions, but SyrNN has an additional antiparallel stacking contact between nitronylnitroxide NO groups that qualitatively and computationally is expected to induce antiferromagnetic (AFM) exchange between SyrNN molecules. Experimentally, the magnetism of SyrNN shows evidence of multiple exchange interactions with overall low dimensional AFM exchange behavior. Fits of dc magnetic susceptibility versus temperature data for SyrNN to AFM 1-D chain and 2-D square planar models give $J/k \sim (-)1-3$ K.

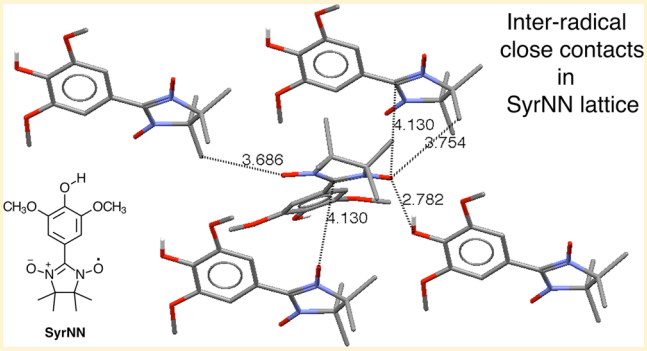

INTRODUCTION

Hydrogen bonding is an important interaction to control intermolecular packing of molecule based electronic materials, including[1] magnetic materials. The magnetic exchange interactions between unpaired electrons in an organic solid can vary quite subtly with only modest changes in intermolecular arrangement. Early efforts attempted to identify simple, spin-orbital-overlap geometric models for predicting magnetic behavior in organic molecular solids,[2] but further study has shown that that these can be quite misleading,[3] save for cases of close (<4 Å) direct spin−orbital overlap between sites with large magnitude spin densities. Relatively sophisticated computational modeling based on experimental crystal structures has given good agreement with experimental magnetic behavior in some cases,[4] but experimental correlation of crystal packing with magnetic behavior remains important for identification of structure−property relationships for organic molecule based magnetic materials.

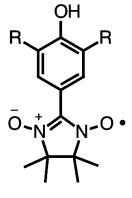

HOPhNN R = H
diBPNN R = t-butyl
SyrNN R = OCH_3

Magnetostructural relationships in the phenolic nitronylnitroxide HOPhNN have been much studied.[5] Its magnetic properties may be linked to exchange via OH to ON hydrogen bonds in its crystal structure, but the spin density on its OH group is known to be quite small for a possible exchange contact site. The analogue diBPNN also forms hydrogen-bonded chains, but with different OH to ON chain contact geometry due to steric hindrance from *tert*-butyl groups flanking the OH group.[6] HOPhNN and diBPNN exhibit ferromagnetic (FM) and antiferromagnetic (AFM) magnetic exchange behavior, respectively. The difference invites the question of what crystallographic differences yield the different magnetic behavior. As part of investigations of these structure−property relationships, we report the synthesis of 2-(3′,5′-dimethoxy-4′-hydroxyphenyl)-4,4,5,5-tetramethyl-4,5-dihydro-1*H*-imidazole-1-oxyl (SyrNN, for "syringyl nitronylnitroxide") and compare its magnetostructural behavior to those of HOPhNN and diBPNN. As we describe below, SyrNN, which lacks the steric hindrance of diBPNN, forms similar OH to ON chains to those of HOPhNN but shows different magnetic behavior due to additional important intermolecular contacts.

Received: November 1, 2012
Revised: December 10, 2012
Published: December 24, 2012

dx.doi.org/10.1021/cg301601c | *Cryst. Growth Des.* 2013, 13, 893−900

Scheme 1. Synthesis of SyrNN

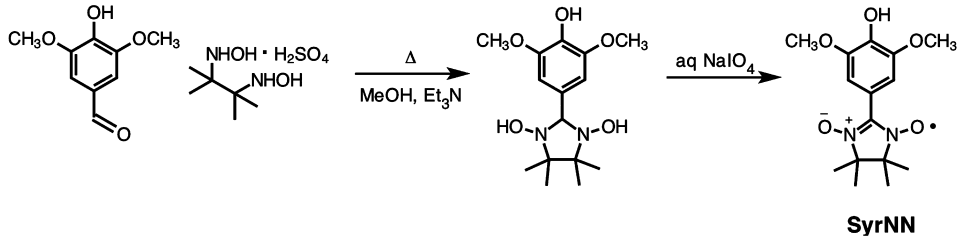

SyrNN

METHODS

Synthesis. SyrNN was made[7] by condensing 2,3-bis-(hydroxylamino)-2,3-dimethylbutane hydrogensulfate with syringaldehyde, and then immediately oxidizing the isolated bis(hydroxylamine) precursor with aqueous $NaIO_4$ at room temperature as shown in Scheme 1. The desired, deep blue nitronylnitroxide can be challenging to isolate due to formation of a red impurity that shows additional peaks in the EPR spectrum beyond those described below for SyrNN. We obtained best results for larger scale oxidization step reactions by the dropwise addition of the oxidizing agent at 0 °C. The crude product was swiftly isolated, subjected to column chromatography, and then crystallized by evaporation from ethyl acetate. On extended standing in solution, the crystallization was sometimes accompanied by formation of red crystallites that show extra EPR peaks beyond those of SyrNN. We suspect that the red impurity is the iminoylnitroxide analogue of SyrNN but were not able to prove this by purifying the byproduct away from accompanying nitronylnitroxide. Fortunately, we found that the red byproduct crystallites could typically be manually separated from the dark blue, pure crystals of SyrNN.

Crystallography. A single crystal of SyrNN was selected and analyzed using a Bruker Nonius KappaCCD instrument. Data work up was carried out using[8] SHELXTL 97. ORTEP diagrams were generated with ORTEP 3 (v2.02) for Windows;[9] crystal packing diagrams were generated using the Cambridge Crystallographic Data Centre program Mercury (v3.0.1).[10]

Magnetic Measurements. For measurements at 1.8 K and higher temperatures, polycrystalline samples of SyrNN were placed in gelatin capsules and held in place with a small plug of cotton. The capsules were placed in a sample holder stick for a Quantum Design MPMS-5 magnetometer, purged with helium, and cooled for magnetization versus field (M vs H) measurements at 1.8 K, and variable temperature dc magnetic susceptibility (χ) measurements at an external fields of 100 and 1000 Oe. Raw susceptibility values were corrected for diamagnetic and sample holder contributions by extrapolation of the high temperature data. The dc-χ values at the two different fields were essentially the same, so only the 1000 Oe results are shown throughout this article, unless explicitly described otherwise.

For measurements below 1.8 K, magnetization versus field and temperature were carried out using a custom built[11] vibrating sample magnetometer in a ^{3}He refrigerator system. Ac magnetic susceptibility measurements were performed[11] in a ^{3}He refrigerator system, using the mutual inductance coil technique with operation at 155 Hz frequency and 10 Oe modulation field.

RESULTS AND DISCUSSION

Polycrystalline SyrNN shows a relatively broad OH stretching band in the infrared spectrum, indicative of hydrogen bonding that was confirmed by crystallography as described later. Its room temperature solution EPR spectrum in toluene has g = 2.0068 with pentet 1:3:5:3:1 hyperfine splitting characteristic of two equivalent nitrogen atoms, a_N = 7.56 G; additional hyperfine is resolved in the higher field peaks, attributed to the nitronylnitroxide methyl groups with a_H = 0.27 G. The EPR results are important, because they clearly show observable spin density to be present on the nitronylnitroxide methyl groups, which thereby can play a role in intermolecular exchange interactions.

SyrNN forms blue-black prisms that are quite stable to ambient conditions once isolated as a solid, despite some instability in solution. X-ray diffraction (XRD) results from the single crystal analysis are summarized in Table 1. Figure 1 schematically shows three magnetically important intermolecular contacts in the structure: hydrogen bonded OH···O−N chains, inter-radical chain contacts involving direct SOMO−SOMO interactions, and interadical CH_3···ON contact chains. The proposed roles that these play in SyrNN magnetism are discussed below.

Table 1. Summary of the Crystal Structure Data Collection and Refinement Parameters for SyrNN[a]

compound	(1)
empirical formula	$C_{15}H_{21}N_2O_5$
formula weight (g·mol^{-1})	309.34
temperature (K)	293
wavelength (Å)	0.71073
crystal system	monoclinic
space group	*Cc*
a (Å)	14.2986(5)
b (Å)	14.2986(5)
c (Å)	9.8965(2)
β (°)	123.1518(16)
volume (Å^3)	1611.86(9)
Z	4
calculated density (g cm^{-3})	1.275
absorption coefficient (mm^{-1})	0.096
F(000)	660
θ range (°)	4.49−25.03
index ranges	h = −16→16
	k = −16→16
	l = −11→11
reflections collected	2714
independent reflections	5318 [R(int) = 0.03]
data/restraints/parameters	2714/2/202
goodness-of-fit on F^2	1.058
final R indices [$I > 2\sigma(I)$]	R_1 = 0.034 (2592)
	wR_2 = 0.0916 (2592)
R indices (all data)	R_1 = 0.0368
	wR_2 = 0.0937
$\Delta\rho_{min}$, $\Delta\rho_{max}$ (e Å^{-3})	−0.12, 0.15

[a] $w = 1/[\sigma^2(F_o^2) + (0.0560P)^2 + 0.351P]$, where $P = (F_o^2 + 2F_c^2)/3$.

The molar magnetization versus field for SyrNN normalized to an expected field-saturated magnetization of 5585 emu/mol for S = 1/2 spin carriers (M/M_s versus H, Figure 2) lies well below the Brillouin curve expected for isolated S = 1/2 spins, indicating significant intermolecular AFM exchange interac-

dx.doi.org/10.1021/cg301601c | Cryst. Growth Des. 2013, 13, 893−900

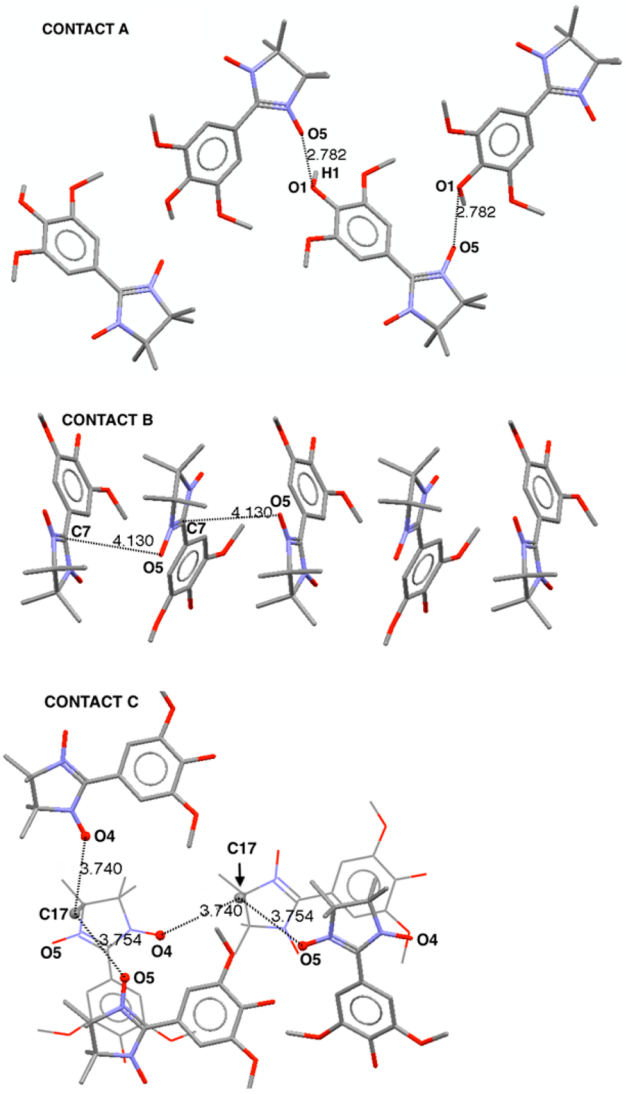

Figure 1. Crystallographic intermolecular contacts involving the SyrNN nitronylnitroxide units: hydrogen bonded OH···O−N chains (contact A), inter-radical N−O···C chain contacts (contact B), radical-methyl CH_3···ON 2-D network (contact C). The wireframe structures in the bottom chart lie below the plane holding the tube-bond structures.

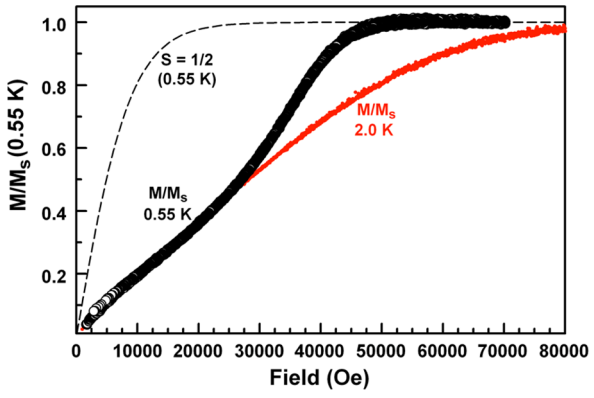

Figure 2. Molar magnetization normalized to saturation magnetization (M/M_s) versus field at 0.55 K (upper, black data) and 2.0 K (lower, red data). The dashed line shows the Brillouin curve expected for isolated $S = 1/2$ spins at 0.55 K.

tions. Figure 2 is nearly linear up to 40 000 Oe at 1.8 K, with a very subtle inflection point at ~7000 Oe detectable in a second derivative plot (see Supporting Information). At 0.55 K, M/M_s versus H becomes more complicated, with a concave down region from the minimum measured 1000 to 7000 Oe, a concave up region from 7000 to 40 000 Oe, then a concave down region above 40 000 Oe that saturates by ~50 000 Oe. A semilog plot (Supporting Information) also shows three M/M_s versus H regions: a rapid rise lower field region, a slower rise midfield region, and the saturation region (see Supporting Information). In a mean field approximation,[12] $M/M_s = g\mu_B H/2zJ{\cdot}S$ where zJ is the averaged exchange interaction of an $S = 1/2$ unit with z nearest neighbors. The 2 K data of Figure 2 yield $|zJ/k| = 7.7$ K from the slope of the linear region of the plot, using this relationship. Details are given in Supporting Information. This value for exchange is in reasonable agreement with analyses of magnetic susceptibility versus temperature that are described below.

This multiregion M/M_s versus H behavior indicates the presence of multiple exchange mechanisms: the plot shape is consistent with low-dimensional chain or 2-D interactions. So, we considered possibilities for intermolecular exchange in the SyrNN crystal lattice, based on the crystal structure, combined with the SyrNN solution phase EPR-derived and computationally modeled molecular spin density distribution.

B3LYP[13]/EPR-III[14] computations using Gaussian 09[15] for SyrNN at the crystallographic geometry predict hyperfine splittings of $a_H = \pm$ 0.2−0.7 G (0.04−0.1% spin density magnitudes) for the nitronylnitroxide methyl groups, depending on rotational placement. This is in reasonable agreement with experimentally observed small hyperfine of $a_H = 0.27$ G. The observed methyl hyperfine comes from solution dynamic averaging of multiple couplings as the methyl groups rotate and the nitronylnitroxide ring puckers in solution. In the solid state, the spin density on the methyl hydrogens depends on pseudoaxial versus pseudoequatorial methyl group geometry[5b] in the nitronylnitroxide ring. So, it is not straightforward to extrapolate the solution hyperfine to solid state exchange behavior for intermolecular CH_3···ON contacts described later. The phenolic hydrogen is computed to have $a_H = +0.2$ G (0.05% spin density), on the lower end of range of predicted methyl hfc. Similar levels of hybrid DFT computational theory are known to reproduce solution phase EPR hfc in 2-aryl-NNs, with a tendency to underestimate the experimental spin polarization (and, in our experience, the nitrogen hyperfine coupling).[5b,16] A graphical summary of the EPR-III computed spin density distribution in molecular SyrNN is shown[17] in Figure 4.

Solution phase spin density estimates do not necessarily reflect solid state spin density distributions. But solid state NMR studies for HOPhNN have shown[5b] experimentally *similar* magnitude spin densities on OH and methyl groups. Also, computations using isolated molecule models support[16] the similarity of OH and methyl hyperfine constant magnitude in HOPhNN. So, O−H···O−N and C−H(methyl)···O−N contacts could both provide small intermolecular exchange pathways in SyrNN and the related phenoxyl radicals due to the closeness of the contacts and the large spin densities involved on the NO group.

The dc magnetic susceptibility of SyrNN was obtained in separate experiments at 0.6−20 K and 1.8−300 K, and the combined data were plotted as shown in Figure 3. The data were obtained at 1000 Oe, in the nearly linear M vs H region.

dx.doi.org/10.1021/cg301601c | *Cryst. Growth Des.* 2013, 13, 893−900

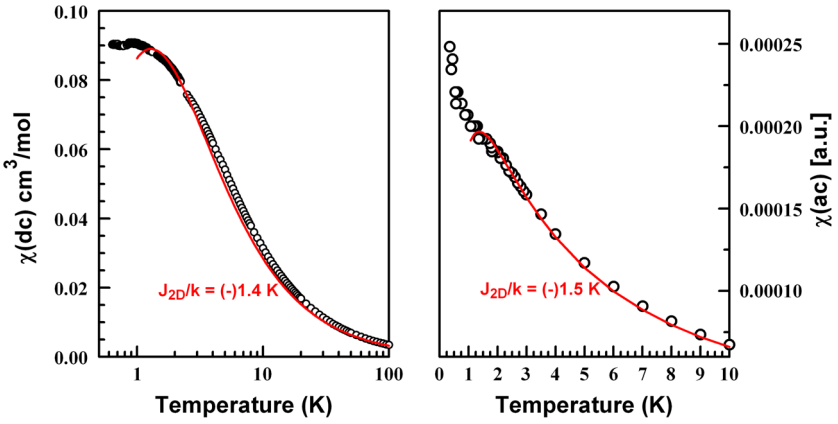

Figure 3. Magnetic susceptibility versus temperature for SyrNN. Left panel shows χ_{dc} versus T data at 1000 Oe external field. Right panel shows χ_{ac} versus T data in zero external field (modulation 10 Oe, frequency 155 Hz). The solid red lines show fits to an AFM 2D square planar model for $T >$ 1 K data without mean field correction.

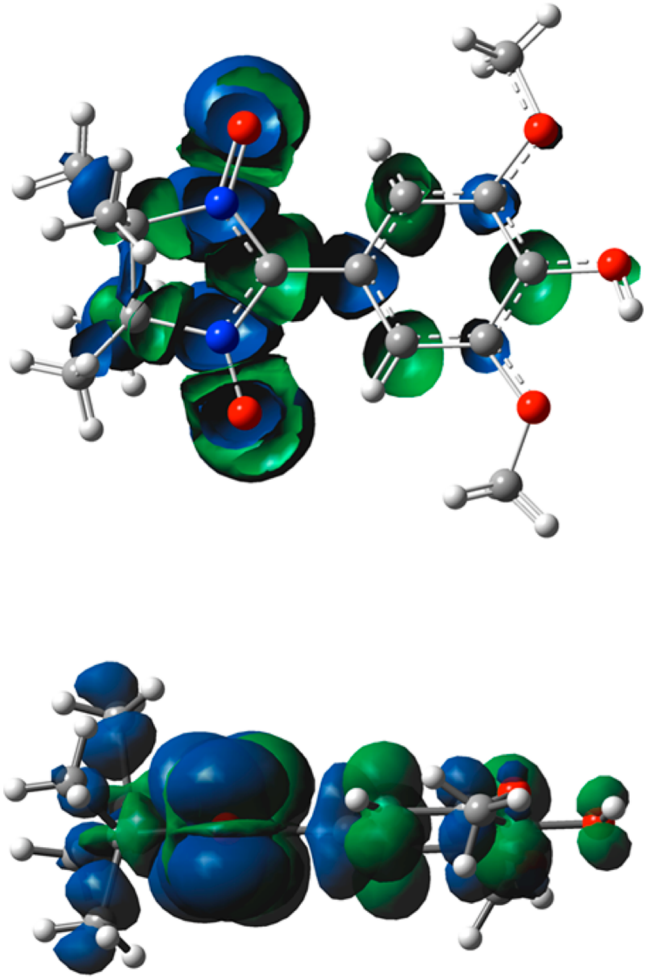

Figure 4. UB3LYP/EPR-III computed spin density distribution in SyrNN from the crystallographic geometry of one molecule, Z-clipped at the approximate plane of the nitronylnitroxide ON-C-NO moiety. The SOMO orbital contour value is 0.02, and the density value is 0.004 for both views.

The χ_{dc} versus T curve lies well below the theoretical isolated-spin $S = 1/2$ Curie curve, indicating AFM exchange. A Curie–Weiss plot of $1/\chi_{dc}$ versus T yields a Weiss constant from the abscissa intercept of $\theta = -1.4$ K from the 1.8–300 K experiment, also indicating AFM exchange (see Supporting Information). Below 4 K, the plot rises monotonically until it levels out below 1.5 K to give an ill-defined maximum at about 0.9 K. A zero field ac susceptibility plot over 0.35–10 K (155 Hz modulation frequency, 10 Oe modulation amplitude) shows χ_{ac} versus T to rise below 4 K, as is also shown in Figure 3. Because there is no maximum in the zero field χ_{ac} versus T plot there is no evidence that SyrNN forms a magnetically ordered state above 0.35 K. The smooth trend in the M vs H data in Figure 2 (no sudden rise) argues against possible metamagnetic behavior, especially given the lack of an antiferromagnetic transition in the χ_{ac} versus T data above 0.35 K.

The χ_{dc} versus T data were fitted to several magnetic exchange models: antiferromagnetic (AFM) spin-pairing,[18] 1-D Heisenberg AFM chain,[19] and 2-D Heisenberg AFM square planar[20] models for $S = 1/2$ spins, with and without a mean field correction θ_{MF}, over the full temperature range and for $T >$ 1 K (because of the change in the data trend for the χ_{ac} versus T data). For all cases, interelectron exchange values are given using the general Hamiltonian $H = -JS_a \cdot S_b$. Table 4 shows the results for the $T > 1$ K fits, which were statistically better, although the J/k values for fitting the full temperature range were similar. Spin-pairing fits gave $J/k < \theta_{MF}$, indicating model inadequacy (see Supporting Information): since SyrNN crystallography does not exhibit inter-radical dyads, this model was not further considered. Both 1-D Bonner–Fisher AFM chain and 2-D AFM square planar models gave relatively good fits for $T > 1$ K even without a mean field term; inclusion of a mean field term improves the fits and somewhat increases the magnitude of J/k in both cases. For all the variations of 1-D and 2-D fitting that were tested, $J/k \sim (-)1.2$–2.9 K. Figure 3 shows the 2-D AFM square planar fits without mean field correction; the J_{2D}/k values obtained by fitting the $T > 1$ K data are nearly the same for both the χ_{dc} and χ_{ac} data. Details of the various fitting results are given in Supporting Information. It is gratifying to note that the estimate of $|zJ/k| = 7.7$ K from the above-described mean field treatment of the Figure 2 magnetization data is quite comparable to the J/k values from the χ vs T fits, if $|J/k| = 1.9$ K and $z = 4$ for the number of nearest neighbor exchange interactions from a 2-D approximation. Still, given the complexity of possible exchange paths from the SyrNN crystallography, these results might be best considered just to support low dimensional AFM exchange in the system.

dx.doi.org/10.1021/cg301601c | Cryst. Growth Des. 2013, 13, 893–900

As part of our effects to identify common or differing magnetostructural relationships among the phenolic nitronylnitroxides, Tables 2 and 3 compare selected molecular and intermolecular geometric parameters for SyrNN to analogous parameters for HOPhNN and diBPNN. SyrNN forms 1-D chains of O1−(H)···O5−N11 contacts, with the O−H donor groups hydrogen bonded directly to large spin density sites on acceptor nitronylnitroxide units at r(O1···O5) = 2.782(2) Å. HOPhNN and diBPNN form analogous O−(H)···O−N chain contacts at distances of 2.67−2.69 Å and 2.88−2.95 Å, respectively; the value for SyrNN thus lies intermediate between these. But steric effects in diBPNN force its O−H group well out of the plane of the phenyl ring to approach the "top" of a radical NO group, in the region of its singly occupied molecular orbital (π-SOMO). Previous computational work indicates that the bent hydrogen bond contact A in diBPNN favors AFM exchange.[6] This is different from the case in both HOPhNN and SyrNN, where the OH groups lie nearly in the plane of their phenyl rings, as shown in Scheme 2. The HOPhNN and SyrNN OH groups point toward NO group lone pairs to give shorter, stronger, S-ribbon shaped hydrogen bonded chains than the twisted diBPNN OH···ON chains; the linear hydrogen bond geometry has been computed to favor[6] FM exchange.

Table 2. Molecular Structure Parameters for SyrNN Compared to Analogous Values for HOPhNN, diBPNN

compound	SyrNN	HOPhNN	diBPNN
N−O bond lengths	1.281, 1.285	1.274, 1.283	1.275, 1.291
		1.275, 1.289	1.276, 1.291
			1.299, 1.276
ON−C−NO bond lengths	1.349, 1.349	1.341, 1.363	1.350, 1.333
		1.331, 1.361	1.340, 1.347
			1.326, 1.352
aryl−NN connecting bond length	1.462	1.452	1.452
		1.444	1.450
			1.453
aryl−O(H) bond length	1.359	1.360	1.361
		1.368	1.359
			1.357
aryl−NN dihedral angle[a]	16.47°	32.67°	35.41°
		33.57°	35.25°
			31.26°

[a]Plane-plane angle using all carbon atoms of pyrene and the ONCNO atoms for the nitronylnitroxide unit.

Scheme 2. Linear and Bent Hydrogen Bonds in Phenolic Nitronylnitroxides

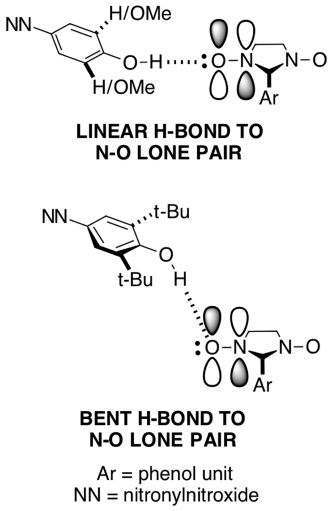

All three systems have multiple radical NO to radical methyl group contacts that form chains or sheets. As described earlier, these contacts are plausible sites for exchange, given the nonzero spin densities on the methyl groups. Since they are present in all of the molecular crystals, their magnetic exchange effects may vary in magnitude but seem likely otherwise to make qualitatively similar contributions to all of these phenolic nitronylnitroxides.

But a major difference between SyrNN and the other two is that *only* SyrNN forms stacked radical−radical contacts at just about 4 Å distance, shown in contact B of Figure 1. This is a moderately long inter-radical contact for second row element radical sites, but it occurs between sites bearing the largest spin densities in SyrNN. Also, the contact B inter-radical geometry forces direct SOMO−SOMO contact, making this an effective exchange pathway for SyrNN. As shown in Table 3, HOPhNN and diBPNN lack analogous B-type contacts between nitronylnitroxide units, so their exchange behavior is most likely to be controlled by A and C type contacts.

The exchange interactions between closest contacts in the SyrNN lattice were computationally modeled using intermolecular dyads at crystallographic geometries. Using method-

Table 3. Selected Intermolecular Contacts for SyrNN Compared to Analogues for HOPhNN, diBPNN[a]

compound	SyrNN	HOPhNN[b]	diBPNN[c]
O(H)···O−N (contact A type)	2.782 [O1(H)···O5]	2.67, 2.69	2.88, 2.90, 2.945
contact A computed exchange	−0.06 K	+0.63 K[d]	−0.16 K[d]
closest N−O to N−O approach	3.993 [O5···N8′]	4.76	5.58, 5.62
N−O···C(NO)$_2$ (contact B type)	4.130 [O5···C7′]	4.63	n/a
contact B computed exchange	−0.82 K		
C(H)$_3$···O−N (contact C type)	3.754 [C17′···O4″][e]	3.35−3.51	3.27−3.73
	3.740 [O5···C17′]		
	3.686 [C15···O4‴]		
	3.740 [C17···O4‴]		
contact C computed exchange	−0.82 K[e]		

[a]All distances in angstroms. [b]From Cambridge Structure Database crystal structure HAFXOB, ref 5c. [c]From Cambridge Structure Database crystal structure SAKWAD, ref 6. [d]From ref 6. [e]Contact B for SyrNN includes this NO to methyl contact; other variatiants of the contact C yield smaller magnitude exchange values. The computed exchanges would also vary by the rotameric placement of C−H bonds in the methyl group.computed.

dx.doi.org/10.1021/cg301601c | Cryst. Growth Des. 2013, 13, 893−900

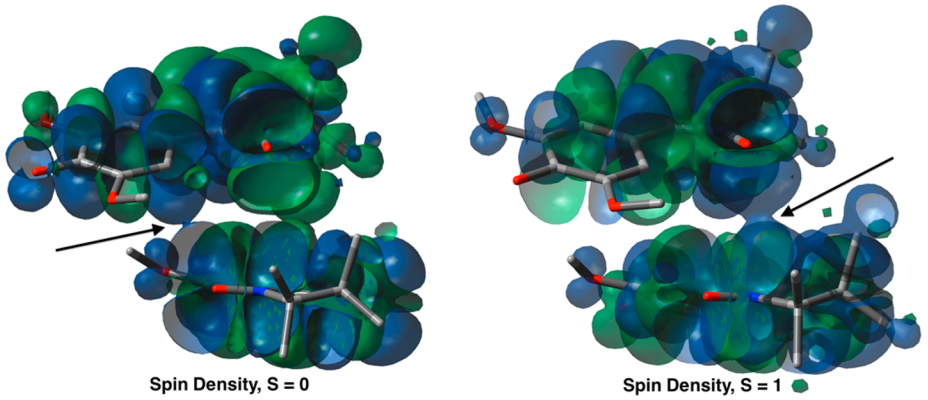

Figure 5. UB3LYP/6-31G* computed spin density distributions for contact A (N−O to N−O) dyad geometry in crystalline SyrNN (see Figure 3, Table 3). The left graphic shows lower energy low spin state; the right graphic shows the high spin state. The views are Z-clipped to visualize more easily the points of contact (arrows) between radical sites. Red = oxygen atoms.

ology similar to that used by Novoa for exchange modeling in similar systems,[4] hybrid density functional UB3LYP[13]/6-31G* computations in Gaussian 09[15] were used. Singlet state energies were computed with broken-symmetry wave functions, and triplet-singlet energy differences were corrected for the spin contamination in the singlet computations by using Yamaguchi's method[21] in eq 1, where $<S^2>$ are spin expectation values, and HS/LS signify high-spin and low-spin states, respectively:

$$\Delta E_{T-S} = \frac{E_S - E_T}{<S^2_{HS}> - <S^2_{LS}>} \quad (1)$$

Table 3 shows the computed exchange interaction values for the O(H)···O−N contacts A in all three compounds, and contact B between nitronylnitroxide units in SyrNN. Analogous contact B distances in HOPhNN and diBPNN are too long to give significant exchange interactions. The SyrNN contact B gives a slightly larger magnitude ΔE(T−S) among these, a negative AFM exchange value. Figure 5 shows the contact B interaction as a spin density diagram at the crystallographic dyad geometry, for both the low spin $S = 0$ and high spin $S = 1$ UB3LYP/6-31G* computations. The points of contact between the radicals in this geometry are readily seen, although these shift somewhat between the spin states due to associated movement of spin density (α- versus β-spin) nodal surfaces.

Taylor and Lahti previously suggested based on computational modeling that HOPhNN should have an FM exchange interaction across the hydrogen bonding contact A.[6] This suggests that contact A is important in causing HOPhNN to be the only one of these phenolic radicals that has experimentally observed FM exchange behavior (see Table 4). The SyrNN contact A is not as linear as in HOPhNN. The SyrNN nitronylnitroxide acceptor O5′ forms a dihedral angle of 9.3° relative to the phenolic O(H) triad O1−C1−C6, because the acceptor NO group lies a bit above the plane of the phenol. The analogous out-of plane tilt in the two forms of HOPhNN is only 4.9° and 6.5°. The difference may account for SyrNN having a small and qualitatively AFM computed contact A exchange, by comparison to the structurally analogous contact having computed FM exchange in HOPhNN. The computations for the small magnitude contact A exchange are consistent with the experimental observations, albeit that one must always consider the dangers of overemphasizing one such magneto-structural relationship[3,4] among a set of multiple competing, small exchange interactions.

Table 4. Results of Fitting SyrNN Magnetic Susceptibility versus Temperature Results to Various Models[a]

model	J/k (θ_{MF}), $T > 1$ K	J/k (θ_{MF}), all data
SyrNN 1-D AFM chain[b]	−2.04 K	−1.80 K
	−2.92 K (θ = +0.31 K)	−2.46 K (θ = +0.18 K)
SyrNN 2-D square planar[c]	−1.38 K	−1.17 K
	−2.19 K (θ = +0.45 K)	−1.79 K (θ = +0.30 K)
HOPhNN 1-D AFM chain	+2.02 K (θ = −0.54 K)[d]	
HOPhNN 2-D AFM sheet	+1.26 K (θ = −1.12 K)[d]	
diBPNN 1-D AFM chain	−6.08 K (θ = −0.38 K)[e]	

[a]Upper numbers for fits with $T > 1$ K, lower numbers for fits with all data. Comparison literature experimental results are given for HOPhNN and diBPNN. All exchange constants J/k reflect a general hamiltonian $H = -J_{ab}S_a \cdot S_b$; $J < 0$ reflects antiferromagnetic exchange; θ_{MF} is a mean field parameter where used. [b]Bonner−Fischer model of ref 18. [c]2-D model of ref 19. [d]From ref 5a; values doubled from those reported for comparison to the Hamiltonian used in this article. [e]From ref 6; values doubled from those reported for comparison to the Hamiltonian used in this article.

If contacts A do influence heavily the qualitative behaviors of HOPhNN, SyrNN, and diBPNN, quantitatively the magnitude of the AFM exchange reported by Taylor and Lahti in diBPNN (Table 4) is harder to explain. But other contacts can make contributions to the overall behavior, of course. Since diBPNN has some of the closest contact C type CH_3···ON contacts among the three phenolic nitronylnitroxides, these may play a key role in giving diBPNN a more sizable AFM exchange by reinforcing the exchange effect of the uniquely bent diBPNN OH···ON contact A shown in Scheme 2.

Finally, both ac- and dc-susceptibility behavior in SyrNN below about 0.5 K suggest that a small FM exchange interaction is present, in addition to the larger, low dimensional AFM exchange interactions. This rise in lowest temperature magnetic χ vs T data may arise from small changes in the stacking geometry during cooling, which could move the nitroxide O5 more directly over neighboring C7 in the contact B chains of Figure 1; this would favor FM exchange interaction. In addition, as shown in Table 3, there are multiple contact C type CH_3···ON contacts. One of these is computed to yield a slight FM exchange interaction (not listed in Table 3, but given

in Supporting Information as contact C2). The magnitude of the smallest computed exchange here is such that one should not trust too strongly in its being a significant contributor to the overall magnetic behavior. While changes in computed exchange magnitudes (and possibly even sign of exchange for the smallest interactions) will likely occur if other basis sets or functionals were used to compute the exchange, in a larger sense the small exchange energies computed here demonstrate the subtleties of trying to model effects of small geometry changes upon overall magnetic behavior. Either small lattice changes any specific $CH_3\cdots ON$ contacts are somewhat speculative individual contributors to the multiple exchange interactions suggested by the magnetization behavior in Figure 2.

CONCLUSIONS

A new, stable nitronylnitroxide radical with a phenolic hydrogen bonding substituent, SyrNN, was synthesized and characterized by crystallography and magnetic measurements. It forms hydrogen bonded intermolecular chains involving both the phenolic OH and radical NO groups. Although this chain motif is similar to that formed in structurally related HOPhNN that exhibits ferromagnetic exchange behavior at low temperatures, SyrNN shows low dimensional *anti*ferromagnetic exchange behavior, with evidence of multiple exchange mechanisms (though no overall bulk magnetic ordering). The different magnetostructural behaviors of SyrNN and HOPhNN are attributed to the presence of intermolecular chain interactions directly between nitronylnitroxide groups in SyrNN, which are not present in HOPhNN. So, although the hydrogen bonding pattern of the less substituted HOPhNN system is retained in SyrNN, additional contacts form in the latter that influence its overall magnetic behavior. Because of the apparent balance of interactions in SyrNN, this radical may be a candidate for magnetostructural tuning by applied external pressure,[22] or by cocrystallization[23] with other phenolic nitronylnitroxides.

ASSOCIATED CONTENT

Supporting Information

For SyrNN: synthetic details, FTIR and solution EPR spectra, crystallographic information including a summary in CIF format, magnetic analysis details for fitting to various models, computational molecular spin density (with SOMO and spin density diagrams) and crystallographic dyad intermolecular exchange coupling summaries. This material is available free of charge via the Internet at http://pubs.acs.org.

AUTHOR INFORMATION

Corresponding Author

*E-mail: lahti@chem.umass.edu (P.M.L.), freitas@if.usp.br (R.S.F.).

Notes

The authors declare no competing financial interest.

ACKNOWLEDGMENTS

This work was supported by the National Science Foundation under Grant CHE 0809791 (GS, PML, all UMass work). R.S.F. thanks the Fundação de Amparo à Pesquisa do Estado de São Paulo, Brazil (FAPESP - 07/50968-0) for support (sub 2 K magnetic measurements). G.S. thanks FAPESP for support of her collaborative work at the Universidade de São Paulo Instituto de Física. We thank Prof. C. P. Landee for providing us with his expression for fitting the magnetic susceptibility versus temperature behavior of an antiferromagnetic square planar Heisenberg system of $S = 1/2$ spins.

REFERENCES

(1) (a) Cirujeda, J.; Hernandez-Gasio, E.; Lanfranc de Panthou, F.; Laugier, J.; Mas, M.; Molins, E.; Rovira, C.; Novoa, J. J.; Rey, P.; Veciana, J. *Mol. Cryst. Liq. Cryst. Sci. Tech., Sect. A* **1995**, *271*, 1−12. (b) Maspoch, D.; Domingo, N.; Ruiz-Molina, D.; Wurst, K.; Tejada, J.; Rovira, C.; Veciana, J. *Compt. Rend. Chim.* **2005**, *8*, 1213−1225. (c) Lahti, P. M. Magneto-structural Correlations in π-Conjugated Nitroxide-based Radicals: Hydrogen-bonds and Related Interactions in Molecular Organic Solids. In *Carbon-Based Magnetism: An Overview of the Magnetism of Metal-Free Carbon-Based Compounds and Materials*; Palacio, F.; Makarova, T., Eds.; Elsevier: Amsterdam, Netherlands, 2006; pp 23−52. (d) Lahti, P. M. Structure-Property Relationships for Metal-free Organic Magnetic Materials. In Richard, J. P., Ed.; *Adv. Phys. Org. Chem.*; Elsevier: Amsterdam, Netherlands, 2011; Vol. *45*, pp 93−169.

(2) (a) McConnell, H. M. *J. Chem. Phys.* **1963**, *39*, 1910−1911. Cf also discussions in: (b) Yoshizawa, K. Orbital Interactions Determining the Exchange Effects in Organic Molecular Crystals. In *Magnetic Properties of Organic Materials*; Lahti, P. M., Ed.; Marcel-Dekker: New York, 1999; p 377; (c) Yamaguchi, K.; Kawakami, T.; Oda, A.; Yoshioka, Y. MO-Theoretical Elucidation of Spin Alignments in Organic Magnetic Crystals. In *Magnetic Properties of Organic Materials*; Lahti, P. M., Ed.; Marcel-Dekker: New York, 1999; p 403.

(3) (a) Cirujeda, J.; Vidal-Gancedo, J.; Juergens, O.; Mota, F.; Novoa, J. J.; Rovira, C.; Veciana, J. *J. Am. Chem. Soc.* **2000**, *122*, 11393−11405. (b) Deumal, M.; Cirujeda, J.; Veciana, J.; Novoa, J. J. *Chem.—Eur. J.* **1999**, *5*, 1631−1642. (c) Amabilino, D. B.; Cirujeda, J.; Veciana, J. *Philos. Trans.: Math, Phys. Eng. Sci.* **1999**, *357*, 2873−2891.

(4) (a) Deumal, M.; Bearpark, M. J.; Novoa, J. J.; Robb, M. A. *J. Phys. Chem. A* **2002**, *106*, 1299−1315. (b) Jornet, J.; Deumal, M.; Jordi Ribas-Ariño, J.; Bearpark, M. J.; Robb, M. A.; Hicks, R. G.; Novoa, J. J. *Chem.—Eur. J.* **2006**, *12*, 3995−4005. (c) Clarke, C. S.; Jornet-Somoza, J.; Mota, F.; Novoa, J. J.; Deumal, M. *J. Am. Chem. Soc.* **2010**, *132*, 17817−17830.

(5) (a) Cirujeda, J.; Hernàndez-Gasió, E.; Rovira, C.; Stanger, J.-L.; Turek, P.; Veciana, J. *J. Mater. Chem.* **1995**, *5*, 243−252. (b) Heise, H.; Köhler, F.; Mota, F.; Nova, J. J.; Veciana, J. *J. Am. Chem. Soc.* **1999**, *121*, 9659−9667. (c) Hernandez, E.; Mas, M.; Molins, E.; Rovira, C.; Veciana, J. *Angew. Chem., Int. Ed. Engl.* **1993**, *32*, 882−884.

(6) Taylor, P. S.; Lahti, P. M. *Chem. Commun.* **2004**, 2686−2688.

(7) Ovcharenko, V.; Fokin, S.; Rey, P. *Mol. Cryst. Liq. Cryst. Sect. A* **1999**, *334*, 109−119.

(8) Sheldrick, G. M. *SHELXTL97 Program for the Refinement of Crystal Structures*; University of Göttingen: Germany, 1997.

(9) Farrugia, L. J. *J. Appl. Crystallogr.* **1997**, *30*, 565.

(10) (a) Macrae, C. F.; Edgington, P. R.; McCabe, P.; Pidcock, E.; Shields, G. P.; Taylor, R.; Towler, M.; van de Streek, J. *J. Appl. Crystallogr.* **2006**, *39*, 453−457. (b) Macrae, C. F.; Bruno, I. J.; Chisholm, J. A.; Edgington, P. R.; McCabe, P.; Pidcock, E.; Rodriguez-Monge, L.; Taylor, R.; van de Streek, J.; Wood, P. A. *J. Appl. Crystallogr.* **2008**, *41*, 466−470.

(11) Oliveira, N. F., Jr.; Paduan-Filho, A.; Salinas, S. R.; Becerra, C. C. *Phys. Rev. B* **1978**, *18*, 6165−6177.

(12) Kubo, R. *Phys. Rev.* **1952**, *87*, 568−580.

(13) (a) Lee, C.; Yang, W.; Parr, R. G. *Phys. Rev. B* **1988**, *37*, 785−789. (b) Becke, A. D. *J. Chem. Phys.* **1993**, *98*, 5648/1−5648/5. (c) Stephens, P. J.; Devlin, F. J.; Chabalowski, C. F.; Frisch, M. J. *J. Phys. Chem.* **1994**, *98*, 11623−11627.

(14) Barone, V. In *Recent Advances in Density Functional Methods, Part I*; Chong, D. P., Ed.; World Scientific Publishing Co.: Singapore, 1996.

(15) Frisch, M. J., et al. *Gaussian 09*, Revision B.01 ed.; Gaussian, Inc: Wallingford CT, 2010. A full citation is given in the Supporting Information.

(16) Cirujeda, J.; Vidal-Gancedo, J.; Jürgens, O.; Mota, F.; Novoa, J. J.; Rovira, C.; Veciana, J. *J. Am. Chem. Soc.* **2000**, *122*, 11393−11405.
(17) Spin density and orbital maps used in this article and its Supporting Information were generated using Gaussview version 5 for Linux by Dennington, R.; Keith, T.; Millam, J. Semichem Inc.: Shawnee Mission KS, 2009.
(18) Bleaney, B.; Bowers, K. D. *Proc. R. Soc. London, A* **1952**, *214*, 451−465.
(19) Bonner, J. C.; Fisher, M. E. *Phys. Rev.* **1964**, *135*, A640−A658.
(20) Landee, C. P. private communication (2011). See Supporting Information for details of this antiferromagnetic 2-D square planar model.
(21) (a) Yamaguchi, K.; Fukui, H.; Fueno, T. *Chem. Lett.* **1986**, 625−628. (b) Yamaguchi, K. *Chem. Phys. Lett.* **1988**, *149*, 537−542.
(22) For pressure effects on organic radical magnetism, *cf.* the following, and references therein: (a) Takeda, K.; Mito, M. In *Carbon-Based Magnetism: An Overview of the Magnetism of Metal-Free Carbon-Based Compounds and Materials*; Palacio, F.; Makarova, T.; Eds.; Elsevier: Amsterdam, Netherlands; 2006; pp 131−158. (b) Mito, M.; Komorida, Y.; Tsuruda, H.; Tse, J. S.; Desgreniers, S.; Ohishi, Y.; Leitch, A. A.; Cvrkalj, K.; Robertson, C. M.; Oakley, R. T. *J. Am. Chem. Soc.* **2009**, *131*, 16012−16013. (c) Seber, G.; Halder, G. J.; Schlueter, J. A.; Lahti, P. M. *Cryst. Growth Des.* **2011**, *11*, 4261−4266.
(23) (a) Mukai, K.; Suzuki, K.; Ohara, K.; Jamali, J. B.; Achiwa, N. *J. Phys. Soc. Jpn.* **1999**, *68*, 3078−3085. (b) Mukai, K. *Chem. Phys. Lett.* **1999**, *311*, 446−452. (c) Mukai, K.; Yanagimoto, M.; Shimobe, Y.; Kindo, K.; Hamamoto, T. *J. Phys. Chem. B* **2002**, *106*, 3687−3695. (d) Mukai, K.; Yanagimoto, M.; Narimatsu, S.; Maruyama, H.; Narumi, Y.; Kindo, K. *J. Phys. Soc. Jpn.* **2002**, *71*, 2539−2545. (e) Mukai, K.; Yanagimoto, M.; Tanaka, S.; Mito, M.; Kawae, T.; Takeda, K. *Polyhedron* **2003**, *22*, 2091−2098. (f) Mukai, K.; Yanagimoyo, M.; Tanaka, S.; Mito, M. *J. Phys. Soc. Jpn.* **2003**, *72*, 2312−2316. (g) Mito, M.; Tanaka, S.; Kawae, T.; Takeda, K.; Yanagimoto, M.; Mukai, K. *Physica B* **2003**, *329*, 1150−1151. (h) Allen, C.; Haynes, D. A.; Pask, C. M.; Rawson, R. M. *CrystEngComm* **2009**, *11*, 2048−2050. (i) Seber, G.; Freitas, R. S.; Mague, J. T.; Paduan-Filho, A.; Gratens, X.; Bindilatti, V.; Oliveira, N. F., Jr.; Yoshioka, N.; Lahti, P. M. *J. Am. Chem. Soc.* **2012**, *134*, 3825−3833.